Chapter 6

Polyindole functionalized iron inserted-octaethylporphrin: Study of morphology and their electro activity and electronic application

This chapter deals with novel methodology for the synthesis of Polyindole functionalized iron inserted octaethylporphrin (Fe-OEP/PIn). After that, this chapter also describes the structural and morphological properties of Fe-OEP/PIn composite and its application for enhanced electrochemical supercapacitor as well as study of junction behavioral with aluminum contact.

6.1 **Introduction**

Enormous efforts have been endeavored in the direction of development of multifunctional hybrid materials which can simultaneously use for electronics, optoelectronics as well as electrochemical applications [Scott et al. (2007), Peter et al. (1999), Sanchez et al. (2011), Protich et al. (2016)]. The developed organic materials have shown their own potential in different fields from telegrams to touch screen mobiles, smart window, portable electronics devices and energy devices with various advantages such as cost effective, ultrafast response, mobility, good tunable and excellent electro activity. However, the major limitations as processability, stability and low mobility of the organic materials have restricted their applications in devices [Feringa et al. (1993)]. Several conducting polymer (CP) like polyaniline, polypyrrole, polythiophene, polycarbazole etc. [Tiwari et al. (2012), Joshi et al. (2011), Pandey et al. (2013)] have been developed to sort out the issues as for organic materials but still far behind with their inorganic counterparts in respect of charge transport, stability and reliable device performance. Among the various conducting polymers, polyindole and its derivatives have fascinated research community due to their green, biocompatibility, easy in synthesis, low toxicity [Zhijiang et al. (2010), Mishra et al. (2016), Phasuksom et al. (2016)] and potential for various applications such as diode, supercapacitor [Zhou et al. (2016), Raj et al. (2015)], sensor [Kumar et al. (2013)], catalysis etc. [Zhou et al. (2010), Kumar et al. (2013)]. In spite of advantage of PIn over other polymers, the application of PIn is restricted due to various limitations related to conductivity, stability and electro-activity. Therefore, in order to enhance their conductivity as well as electro-activity some manipulation is

needed. In order to achieve this, several methodologies have been employed such as blending with DNA [Hassanien et al. (2010)] as template, nano filler graphene oxide, reduced graphene oxide (GO/rGO), carbon nanotube (CNT) [Dubey et al. (2015), Cai et al. (2016)] etc. in PIn matrix via covalent and noncovalent bonding [Hassanien et al. (2010), Dubey et al. (2015), Cai et al. (2016)]. Recently, development of multifunctional organic materials specially having metal-organic hybrids showed enormous potential for electronics and charge storage applications due to excellent improvement in charge transport properties, stability and electrochemical activity [Forrest et al. (2004), Pandey et al. (2015), Nalwa et al. (1993), Watanabe et al. (2014), Abthagir et al. (2004), Tommie et al. (2004)]. Nowadays, bio-organic molecule, Porphyrin has got tremendous attraction of research community due to its unique electro-activity and optoelectric properties with highly conjugated π electrons, axially ligation capacity to give octahedral M-Porphyrin (L_2) type system. It has also shown promising properties in the area of oxygen reduction reaction (ORR), light harvesting and electronic systems [Wu et al. (2017), Tanaka et al. (2015), Auwarter et al. (2015), Hu et al. (2009)]. Furthermore, porphyrin have shown great potential of stability during functionalization by various groups or molecules through covalent and noncovalent bonding like π-π interactions etc.[Wang et al. (2016), Palacin et al. (2009), Bera et al. (2016), Jahan et al. (2012)]. This stability arises due to its flexible transformation among many forms such as saddle, ruffle, wave, dome [Nurco et al. (1996)]. Several derivatives of porphyrin macrocyclic rings like phthalocyanin (PCn), tetraphenylporphyin of charge or neutral (TPP-OH, TPP-COOH, TPyP etc.) states show solubility in polar solvents but poor in organic solvents. However,

octaethylporphyrin (OEP) is having high solubility in organic solvents due to presence of alkyl groups [Mamardasvili et al. (2000), Paine et al. (1976)]. The planner structure and rich π electron cloud system of OEP introduce a self-aggregation property in itself and with some other molecules also via non-covalent bonding as J aggregation or H aggregation. Therefore, the self-aggregation property of porphyrin may results a new area for engineering of electronic and charge transport properties of organic materials [Hu et al. (2009), Lu et al. (2015), Li et al. (2016)]. It is essential to note that porphyrin shows good affinity towards transition metals like Zn, Co, Ni, Mn, Cu, Fe etc. due to presence of nitrogen hetero atom in central cavity. This results excellent platform for transmit various natural phenomenon like light harvesting and transport of oxygen and electrons. Consequently researchers are interested to mimic an artificial system for facilitating and understanding the process of electro-catalytic activity, optoelectric and electrical properties [Wang et al. (2016), Clement et al. (1998)]. Recently some groups have reported porphyrin or its derivative based electronic devices [Hu et al. (2009)] nanowire [Lu et al. (2015)] organic light emitting diode (OLED) and optoelectronic devices [Ji et al. (2008)]. In order to mimic such a system, various methods are reported for incorporation of metals in porphyrin cavity [Clement et al. (1998), Borghettiet al. (2013)]. However, methods are too complex and take place at elevated temperature. On succession of research in field of composite materials, there are some reports also published based on nano-materials like CNT-Porphyrin [Bera et al. (2016)], graphene-porphyrin [Jahan et al. (2012)], polymer-porphyrin [Itagaki et al. (2005), Paul et al. (2009)] composite with their impact in area of light harvesting, sensor and electro-activity. But there is no any

work published based on Fe- OEP/PIn composite to the best of our knowledge. In this paper, for the first time we present one pot in situ synthesis of a hybrid material of iron inserted octaethylporphyrin/polyindole (Fe-OEP/PIn) in which iron occupies the porphyrin cavity at room temperature and polymerization of indole occurs simultaneously. The ferric chloride ($FeCl_3$) used as oxidizing agent for polymerization oxidizes indole monomer and itself reduces to Fe(II). The Fe(II) has high attraction towards porphyrinic cavity and inserts in the OEP ring under N_2 environment. Various characterization tools like UV–vis absorption, Fourier transform-Infrared (FT-IR), nuclear magnetic resonance (NMR), X-ray photoelectron spectroscopy (XPS), X-ray diffraction (XRD), scanning electron microscopy (SEM), atomic force microscopy (AFM) and Kelvin probe force microscopy (KPFM) are performed to confirm the formation of hybrid material and study of its properties. Initially cyclic voltammetery (CV) was performed to investigate its electrochemical performance which confirmed that Fe-OEP-PIn hybrid possess high electro-activity. Subsequently, the obtained hybrid material is used for fabrication of supercapacitor as well as Schottky diode. The supercapacitor has explored using the GCD and EIS techniques, and Schottky diode using a sandwich structure Al/Fe-OEP-PIn/ITO. Various device parameters including charge transport property and conductivity of the hybrid material are investigated using above sandwiched structure.

6.2 Materials and methods

6.2.1 Materials

Octaethylporphyrin (OEP) and indole monomer was purchased from Sigma-Aldrich, Germeny, and $FeCl_3$ Himedia, India, and used without further purification. Further,

solvent for synthesis such as chloroform, ethanol, Dimethylsulphoxide (DMSO) was purchased from Merck, India and used without further purification however, double distilled water (DDW) used here, was made here and collected from distilled water plant.

6.2.2 Synthesis of PIn:

The polymerization of indole monomer was performed using interfacial method reported somewhere else [Hassanien et al. (2010)]. A 70 mg of indole monomer (60 mmol) was dissolved 10 mL $CHCl_3$ which was colorless solution taken as initial solution. Further, 1mL HCl of 11.4 M was added in this to maintain acidic environment and subsequently whole solution was kept at stirring in N_2 environment for 10 minutes for formation of homogenous solution. Further, 5 mL of aqueous $FeCl_3$ (120 mmol) solution was prepared in vials which was yellowish and added in indole solution as oxidizing agent through glass wall to maintain the interface between organic/aqueous layer. Whole solution was kept in dark place for 2 days and green colour materials PIn appear at interface of organic/aqueous layer which is insoluble in $CHCl_3$ and water. PIn was obtained from the interface by successive removal of water and chloroform. Finally, the obtained PIn was washed three times using DDW and ethanol by successive centrifuge to remove excess $FeCl_3$ and indole monomer and oligomer. Prior to use of materials for characterization and sample preparation, whole material was dried in vacuum oven at 40^oC in dark for one day.

6.2.3 Synthesis of Fe-Porphyrin/PIn composite:

Fe-Porphyrin/PIn composite was synthesized by same route as described above for PIn synthesis. Initially, two necks round bottom flask was collected, washed properly and dried in vacuum oven before using for synthesis of composites. A 70 mg indole monomer (60 mmol) and 97 mg OEP (10 mmol) was dissolved in10 ml $CHCl_3$ contemporarily in presence of N_2 gas in stirring condition. The stirring of solution was conducted only for 5 minutes for formation of homogeneous solution. The obtained solution was used for synthesis of composites. Further, $FeCl_3$ (120 mmol) solution was prepared separately in vials by dissolving 97 mg of $FeCl_3$ in 5 mL DI water for oxidative polymerization. Finally, $FeCl_3$ solution was added carefully to attain the interface (aqueous and non-aqueous interface) into two necks round bottom flask which already contain the OEP and indole monomer solution. The whole contain was kept in dark place for 2 days under inert N_2 atmosphere. Greenness precipitate was obtained at the bottom of flask after two days. This precipitate was extracted by several successive washing in DI water and ethanol followed by centrifuge. The obtained material was dried in vacuum oven at 40^oC for one day.

6.2.4 Synthesis of Fe-OEP

Fe-Porphyrin was synthesized followed same route as described in this (Sun et al. (2011)]. In order to synthesis of Fe inserted OEP, a 100 mL two neck round bottom flask was cleaned and dried it in vacuum oven at 50^oC. Initially, 160 mg of H_2OEP (10 mmol) was added in mixture of acetonitrile and chloroform (20 mL acetonitrile and 10 mL chloroform) respectively in inert environment in stirring condition.

Further, 200 mg of $FeCl_2$ (53 mmol) was added rapidly with care to H_2OEP solution as prepared above. This whole mixture was stirred for half hours at 55ºC in N_2 atmosphere. After this, whole content was cooled upto room temperature at normal cooling rate and subsequently washed by using 5% HCl solution. Furthermore, entire, organic part was collected through separating funnel and dried over anhydrous Na_2SO_4. Finally, the solvent was evaporated by rotatory-evaporator and remaining residue was purified using column chromatography.

6.2 Results and discussion:

6.3.1 Structural analysis

UV-Vis absorption spectra analysis

Figure 6.1 shows the absorption spectra of Fe-OEP, free base OEP, PIn and Fe-OEP/PIn composite. Here, pure H_2OEP absorption spectrum shows one soret band near ultraviolet region at 395 nm and four Q band in the visible region at 499 nm, 530 nm, 565 nm, 620 nm respectively. However, the absorption spectra of H_2OEP have shown visible changes after metalation as shown in inset Figure 6.1(a-b). The soret band is shifting towards lower wavelength contemporarily four Q band converted into two Q band which is consistent with reported in literature [Dolphin et al. (1978)]. The appearance of soret band and Q band can be explained using Gouterman four orbital model, where the free base Porphyrin (H_2OEP) having four orbitals, two highest occupied π* orbital's (HOMO) and two lowest unoccupied π* orbital's (LUMO). The transitions between these levels two HOMOs and two LUMOs was resulting such type of absorbance spectra as shown Figurer 1(a-b). The soret band is arises due to transition between S_0 to S_2 which having high energy and more instance peak however Q band arises due to transition between S_0 to S_1 having less energy and very

low intense peak. Further, metalation of porphyrin causes the transformation of four Q band into two Q band due to shifting in the conjugation pathway and symmetric region viz. transformation of symmetry from D_2h for H_2OEP to D_4h for Fe-OEP. Furthermore study of absorption spectra of PIn shows three band regions. Peak appeared at 295 nm and 375 nm arises due to π-π* transition, n-π* transition however the peak at 398 nm assigned for polaronioc transition which appear due to presence doping during oxidative polymerization [Pandey et al. (2013)]. The absorption spectra of Fe-OEP/PIn composite (Figure 1b) reveals the visible differences on comparison to PIn as well as Fe-OEP separately. A broad peak appears at place of soret band region whereas only two low intense peaks appear at Q band region for iron in OEP cavity. There was some additional peaks at 295 and 350 nm, showing distinguishable feature due to π-π∗, n-π∗ of PIn. The appearance of two Q band and broadening of soret band reveals the metalation of OEP during formation of composite however the noticeable change in spectrum of Fe-OEP/PIn composite as compared to pure PIn and Fe-OEP. The peak at 295 nm are same as pure PIn, yet peak at 375 nm have shifted to 350 nm reveals to change in n-π∗ transition path of PIn. This shift can be justified via interaction between Fe-OEP and PIn through metal centre to nitrogen of PIn.

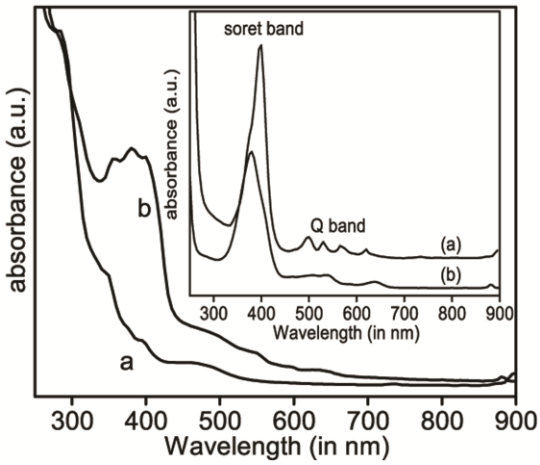

Figure 6.1 UV-vis absorption spectra of (a) Pin (b) Fe-OEP/PIn hybrid, and inset represent the UV-vis absorption spectra of (a) OEP (b) Fe-OEP

FTIR analysis:

For investigation of coordination of iron into OEP cavity and formation of Fe-OEP/PIn composite, FTIR spectrum was recorded from 500 to 3500 cm^{-1} as shown in Figure 6.2. Although, OEP have two N-H group in central cavity which is infrared active and give an intense peak at 3314 cm^{-1}. This peak disappear after binding of metal to central N-H group of OEP, which causes the change in frequency with disappearance of 3314 cm^{-1} and give rise to a qualitative indication for coordination of iron in OEP as shown in Figure 6.2IIa and b. Figure 6.2Ia shows characteristics data of pure PIn as peak at 742 cm^{-1} due to benzene ring C-H bending out of plane indicating benzene ring not participating in polymerization, peak at 1135 cm^{-1} for C-N stretching mode, 1348 cm^{-1} for C-H band, peak at 1400–1600 cm^{-1} due to different C-C stretching mode of aromatic ring and at 3400 cm^{-1} for N-H starching bond and associate with 1598 cm^{-1} for deformation mode of N-H respectively shows that polymerization linkage or coordination of $Fe^{(+2/3)}$ were not via nitrogen [Shuying et al.

(2008), Gupta et al. (2010)]. Further, FTIR spectra of Fe-OEP/PIn (as shown in Figure 6.2Ib) shows visible differences in comparison to pure OEP, and Fe-OEP (*cf.* Figure 6.2Ib and Figure 6.2IIa-b). The peak at 3314 cm^{-1} for N-H vibration of OEP has changed, which clearly indicates the binding of Fe to OEP cavity, and simultaneously some other peaks such as 749, 920, 980 and 1224 cm^{-1} are also appearing which are very sensitive toward metalloporphyrin [Li et al. (2016), Ji et al. (2008)] and again confirmed the coordination of iron in cavity of OEP. Further, a PIn spectrum was investigated (Figure 6.2Ia) and compared with Fe-OEP/PIn hybrid. It was found that there are visible differences as compare to hybrid. Thus, on comparing it was observed that the peak at 3314 cm^{-1} due to N-H bond disappears and significant shift in the four metal sensitive peaks like 749, 920, 1002 and 1224 cm^{-1} concludes that metal iron become doped in porphyrin and appearance of some additional peaks like 3415 cm^{-1} for N-H of PIn in composite confirm the formation of Fe-OEP/PIn composite successfully.

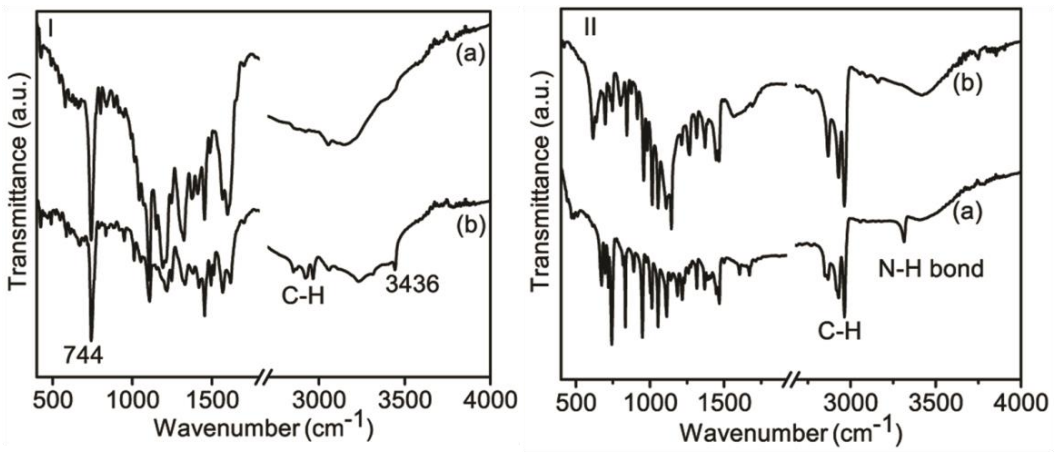

Figure 6.2 FTIR spectra of (Ia) PIn and (Ib) Fe-OEP/PIn composite and (IIa) OEP (IIb) Fe-OEP.

^{1}H-NMR analysis:

In order to interrogate the coordination of iron in porphyrin cavity as well as formation of Fe-OEP/Pin hybrid, ^{1}H NMR experiment was performed as shown in Figure 6.3. Prior to investigation of hybrid material, pure OEP, pure PIn were examined and compared for confirmation of iron coordination as well as formation of Fe-OEP/PIn hybrid material. Figure 6.3a shows the NMR spectra of OEP in $CDCl_3$, a peak near 10 ppm for meso H, 7 ppm ($CHCl_3$ solvent), 4 ppm (-CH_2-proton of ethyl group), 1 ppm (methyl proton of ethyl group), 0 ppm (TMS) and a peak at −4 ppm for N-H proton of free base porphyrin are similar to literature [Xu et al. (2014)]. Further, NMR study of pure PIn in d_6-DMSO as shown in (Figure 6.3c) shows peak at near 10.70 ppm which for the N-H group of indole and also confirms that polymerization is not occurring via nitrogen. Further it also confirms that the nitrogen site is not involve in coordination with $Fe^{(+2/3)}$ ions. In addition to this, peaks appear between 7 and 8 ppm for benzene ring proton [Tiwari et al. (2015)]. Finally, NMR investigation of Fe-OEP/PIn hybrid in d_6-$CDCl_3$ as well as d_6-DMSO as shown in Figure 6.3b, the disappearance of −4 ppm peak for N-H of OEP which is indication of coordination of iron in porphyrin core. A hump at 7–8 ppm region also appears due to presence of benzene ring of PIn however it become clear peaks when d_6-DMSO were used, and a small peak at 10.45 ppm appear for N-H group of PIn. This indicate that some N-H group of PIn do not interact with Fe centre of Fe-OEP and same time, the shifting of peak also happening towards up fields from 10.70 to 10.45 ppm. This type of shifting phenomenon arises due to high electron density experienced by N-H proton of PIn through OEP ring current.

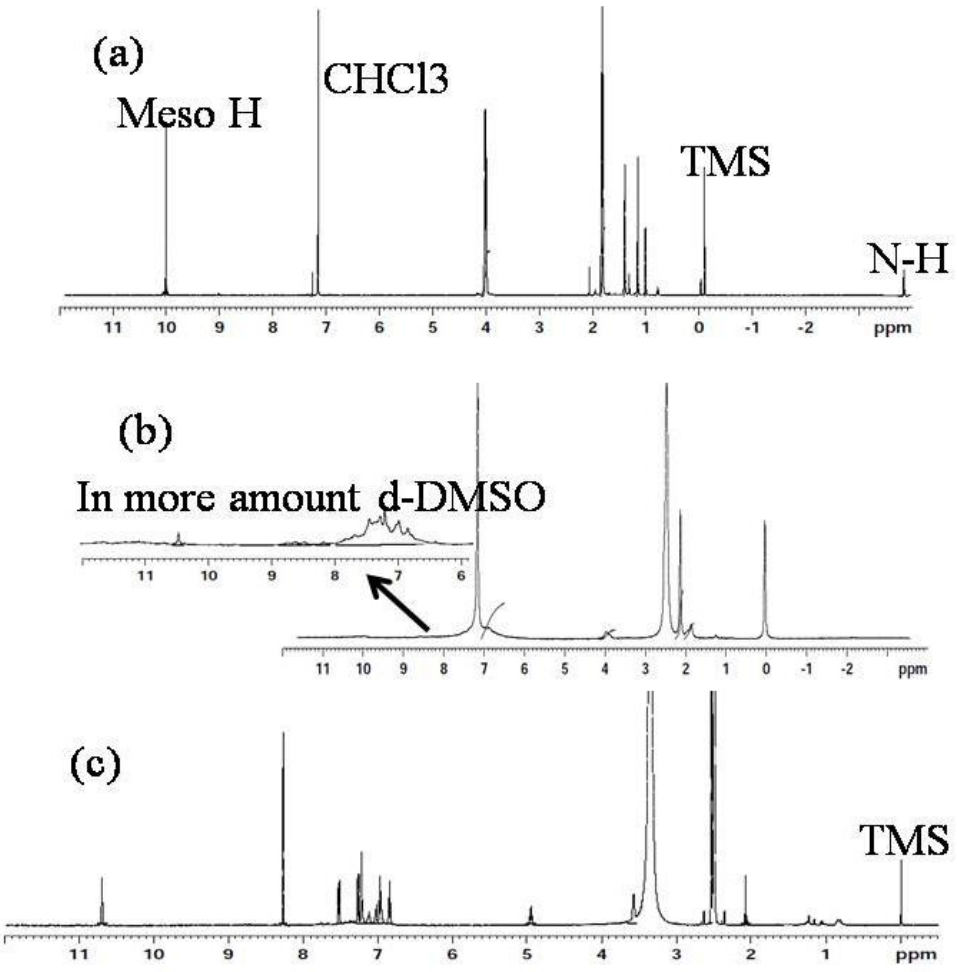

Figure 6.3 H-NMR spectra of (a) OEP, (b) FeOEP/PIn composite and (c) PIn

XRD analysis:

Figure 6.4 presented the structural analysis of (a) OEP,(b) Fe-OEP/PIn hybrid and (c) pure PIn via XRD. The structural analysis of pure OEP shows the diffraction peaks at 10.44, 12.68, 17.28, 17.78, 19.32, 20.16, 28.34, 29.28, 32.38, 34.14, 38.94 as shown in Figure 6.4a. Itis noteworthy that OEP give intense well defined peaks suggested that the formation of ordered and crystalline structure. Further, XRD of as synthesized pure PIn reveal that a broad hump between15° and 40° indicates the formation of

amorphous powder of polymer [Wang et al. (2016), Kumar et al. (2012)] (as illustrated in Figure 6.4c). XRD pattern of Fe-OEP/PIn composite (depicted in Figure 6.4b) reveals both peaks corresponding to Fe-OEP as well as PIn and some additional peaks which absence in either pure Fe-OEP or pure PIn. On comparison of XRD of composite with its parental compound, the peak position as well as their relative intensities was changed from its pure parental compounds. The appearance of new peak discloses the formation of new phase as well as the formation of crystalline structure with instance peaks of Fe-OEP/PIn as compare to pure PIn.

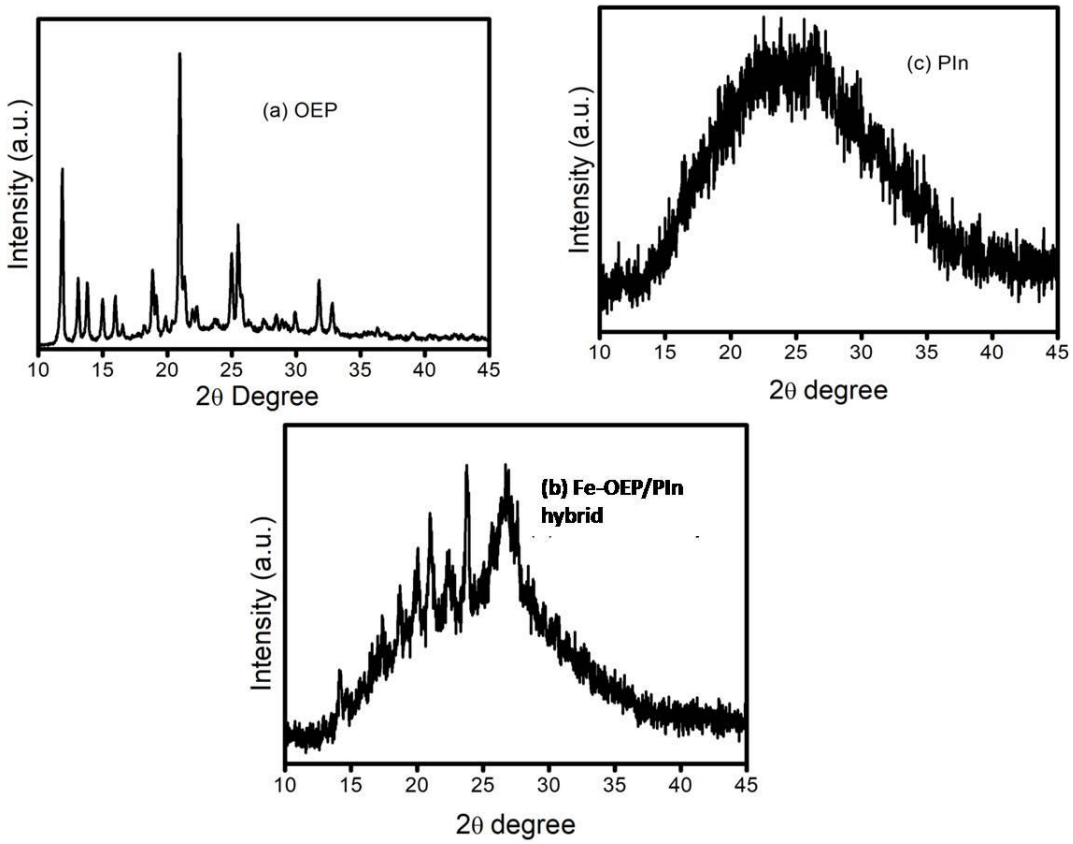

Figure 6.4 XRD spectra of (a) OEP, (b) Fe-OEP/PIn hybrid, and (c) Pure PIn

XPS analysis:

XPS was performed to understand the elemental composition and bonding mode of as synthesized composite. Figure 6.4 illustrates the XPS spectra of C1s, N1s and Fe2p core shell energy level of Fe-OEP and hybrid Fe-OEP/PIn. It is noteworthy here that XPS spectra bestow information about binding energy of core shell of elements where same element in different binding mode gives different binding energy. Our interest was toward interrogation of coordination of iron in OEP and simultaneous formation of Fe-OEP/PIn hybrid. XPS has shown a good way to guide the progress of coordination of iron in porphyrin to show a visible change in the 1s N energy level band. Since OEP has two kinds of N, one pyrrolic (N-H) at higher binding energy (BE) and another called iminic (-N=) at lower BE as reported in literature [Borghetti et al. (2013)]. On coordination of iron, both peaks convert to one band due to all N become chemically equivalent. Figure 6.5Ia illustrate a peak at 399 eV predominated over 401 eV peak which confirms the metalation of OEP. However in Figure 6.5Ib, (b) (corresponding to hybrid) a peak at 401 eV appear as 1s N of PIn [Raj et al. (2015)] are predominant and another band at 399 eV with low intensity for N of coordination of iron in OEP. However, Figure 6.5(II) shows the XPS of C1s corresponding to pure Fe-OEP Fe-OEP/PIn hybrid. In Figure 6.5IIa shows two band at 286 eV and 287 eV were observed for C-C and C-N respectively where as XPS spectra of composite (in Figure 6.5IIb) shows two band, one at 288 eV more intense due to presence of PIn and another is weak band at 286 eV due to porphyrin carbon. XPS spectra was again recorded for Fe 2p core shell energy level for examination of oxidation state of iron metal ion as well as interaction of PIn matrix with Fe-OEP in

composite as shown in Figure 6.5III. The Fe-OEP gives three well resolved peaks at 712.3 eV, 725.3 eV for Fe2p3/2 and Fe2p1/2 respectively and one peak at 718.5 eV (also known as satellite peak) as shown in Figure 6.5IIIa are confirmed the Fe^{3+} state. However hybrid Fe-OEP/PIn shows peak at 712.4 eV for Fe2p3/2 with a small shift, satellite peak shifted to 722.2 eV and Fe2p1/2 peak shifted to726 eV (as shown in Figure 6.5IIIb). On comparison, the spectra reveal that hybrid Fe-OEP/PIn has iron in Fe^{3+} state. These shifts are indicating chemical interaction between Fe-OEP and PIn via metal centre and nitrogen of PIn as also reported in literature [Wang et al. (2016)].

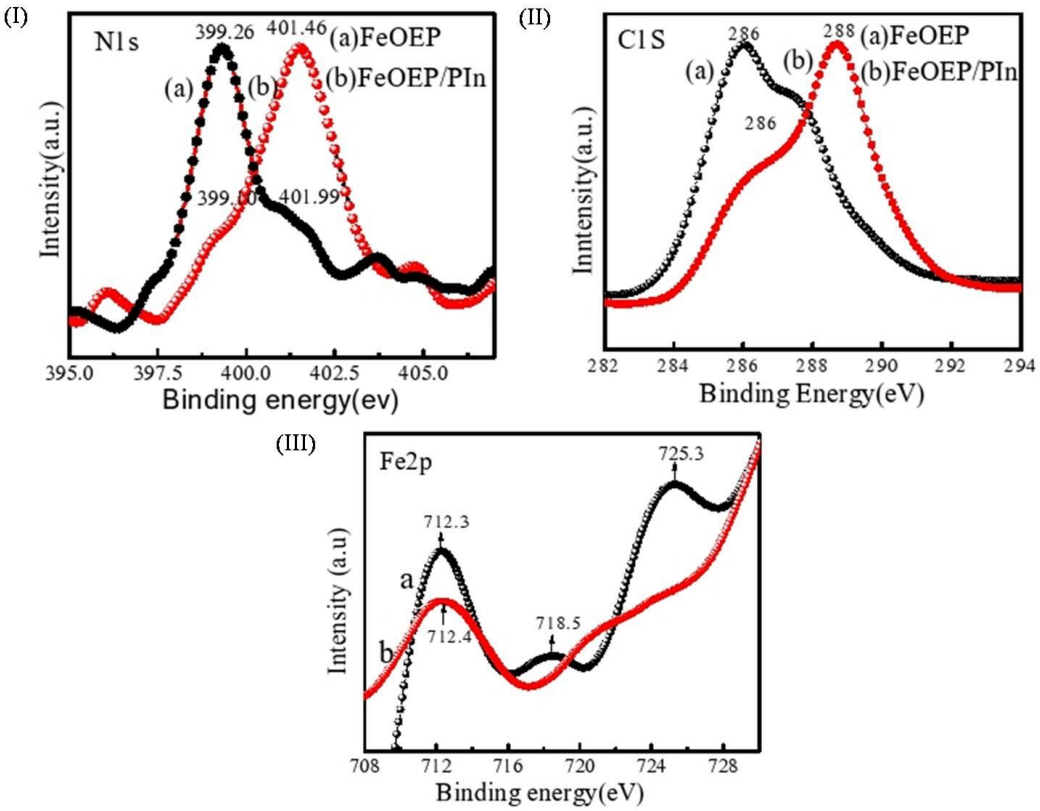

Figure 6.5 XPS spectra of (I) N1s, (II) C1s and (III) Fe2p of corresponding to (a) Fe-OEP, (b) Fe-OEP/Pin hybrid respectively.

On the basis of observed results of FT-IR, NMR, XRD, and XPS, we made scheme for reaction and how PIn and Fe-OEP register in composite (*See* scheme 6.1).The obtained results confirm that Fe insert in OEP and contemporarily indole polymerization take place. The XRD again reveals enhancement in crystalline structure of composite materials.

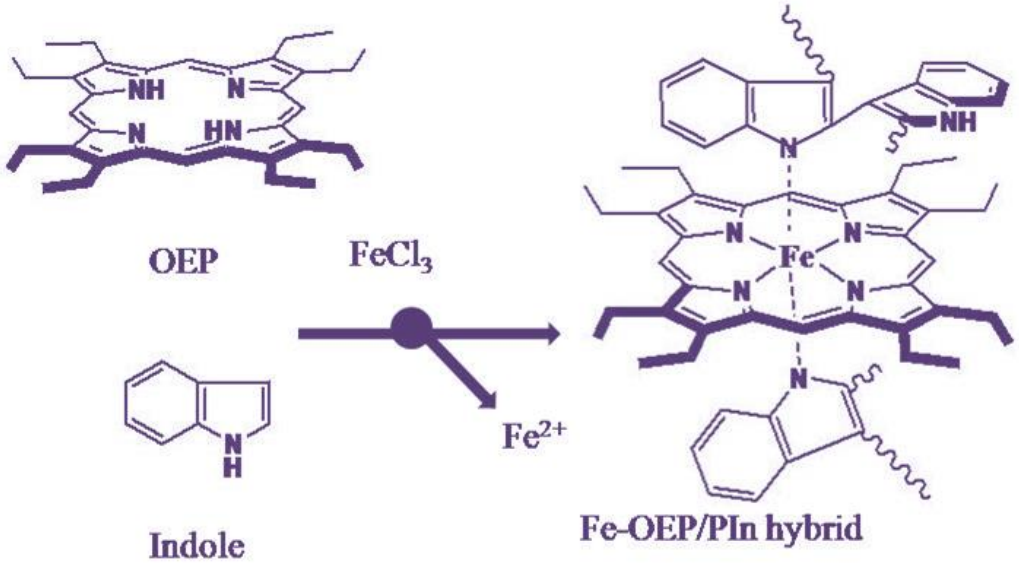

Scheme 6.1 Schematic representation of progress of reaction and interaction between Fe-OEP/PIn.

6.3.2 Morphological analysis:

To realization of surface morphology, roughness, height profile of as synthesized samples the SEM and AFM was recorded. Figure 6.6 a and b) shows a scanning electron microscopy (SEM) image of Fe-OEP/PIn hybrid at different magnifications and compared with pure PIn as shown in Figure 6.6c. Hybrid Fe-OEP/PIn clearly shows the flowery morphology however, pure PIn discloses the bunches of granular

structure. The elemental analysis was further performed via EDX (*See* Figure 6.6(d)) confirmed the presence of Fe in hybrid materials. XRD data also support to such morphology differences because surface properties of materials are directly depend upon phase and orientation of atoms/molecules. The formation of flowery and networks structure in hybrid is indication of formation of connected crystallites. This crystalline nature with flowery shape may enhance the electronic property as well as electro activity of hybrid material.

Surface morphology and surface potential contrast of films are investigated via AFM and KPFM. In order to investigate the AFM topography, KPFM and electronic properties, the as synthesize hybrid was deposited over ITO (conducting glass) via spin coating as described in experimental section. Therefore, prior to study of electrochemical activity and charge transport of hybrid materials, AFM topography, and 3d imaging of PIn and Fe-OEP/PIn hybrid films were conducted over ITO coated glass substrate as shown in Figure 6.7(a, d & b, e). AFM topography of Fe-OEP/PIn hybrid shows very clear difference as compared to pure PIn topography. The Fe-OEP/PIn hybrid shows the globular structure embedded in matrix, however, pure PIn discloses the stretched globular morphology (*cf.* Figure 6.7 (a and b)). The height bar on right side of topography also discloses the dissimilarity. Furthermore, on comparing 3d image of both samples again confirm the more height profile for Fe-OEP/PIn (*cf.* Figure 6.7b and e). In addition to surface morphology and 3d imaging, the surface roughness were also estimated and found around 10 nm and 25 nm for pure PIn and hybrid materials film respectively. Further, the thickness estimation of composite through AFM reveals the formation ~200 nm thick films. In addition to

surface topography, surface potential contrast of composite material were studied using KPFM using Si tip coated with platinum, and compared with pure PIn (as shown in Figure 6.7c and f). It is worth to note that KPFM is based on relative work function measurement of surface relative to tip and measurement of surface potential of PIn and composite film are performed relative Pt coated on Si tip [Pandey et al. (2017)]. Surface potential contrast of composite film shows very plausible difference with change in potential height as well as surface contrast. The differences in potential contrast show the change in electronic property after formation of composite. Composite film shows low relative potential bar, is indication of lowering of HOMO as compare to pure PIn.

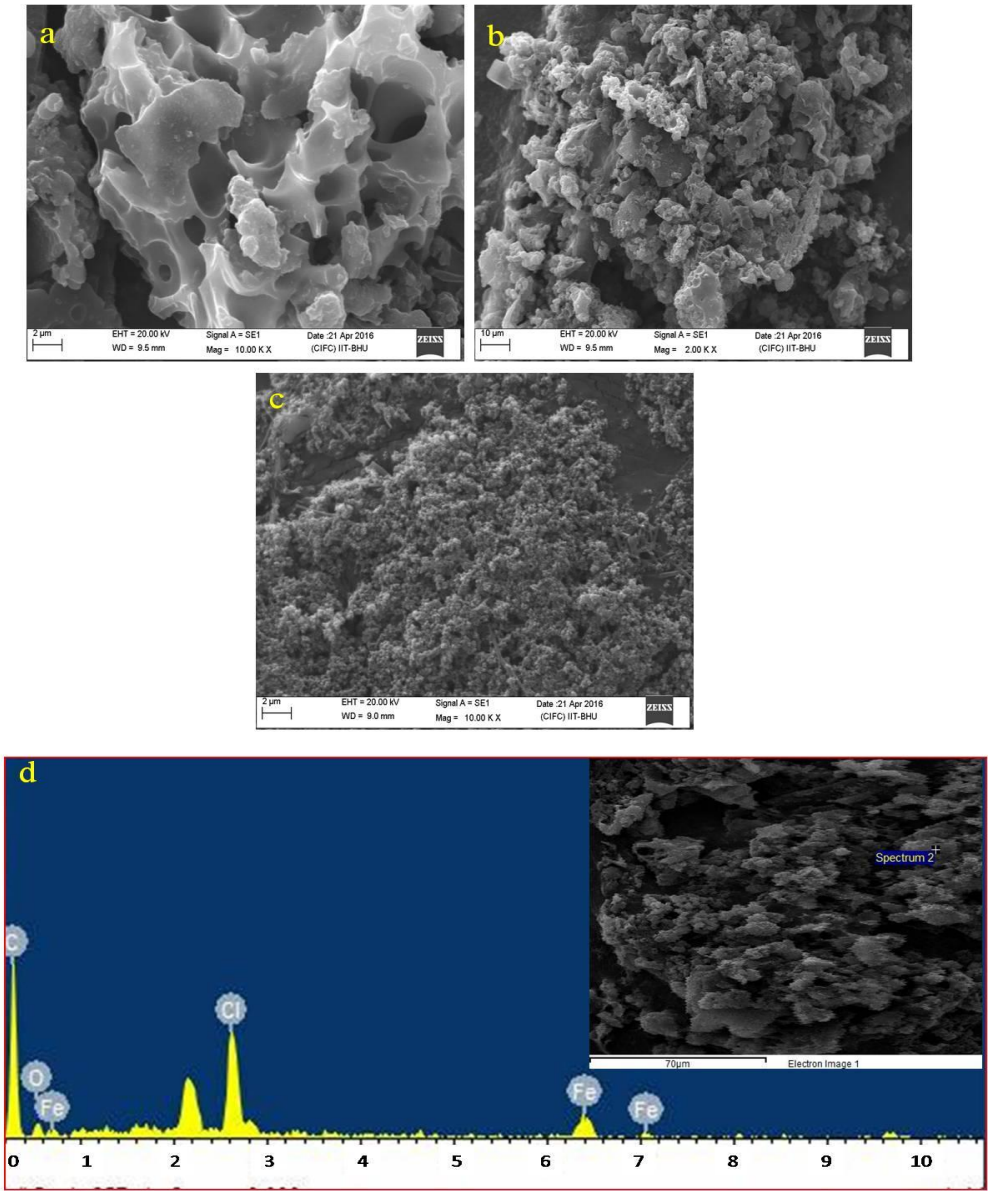

Figure 6.6 SEM of Fe-OEP/PIn at different magnifications (a and b), pure PIn (c) and EDX of Fe-OEP/PIn (d)

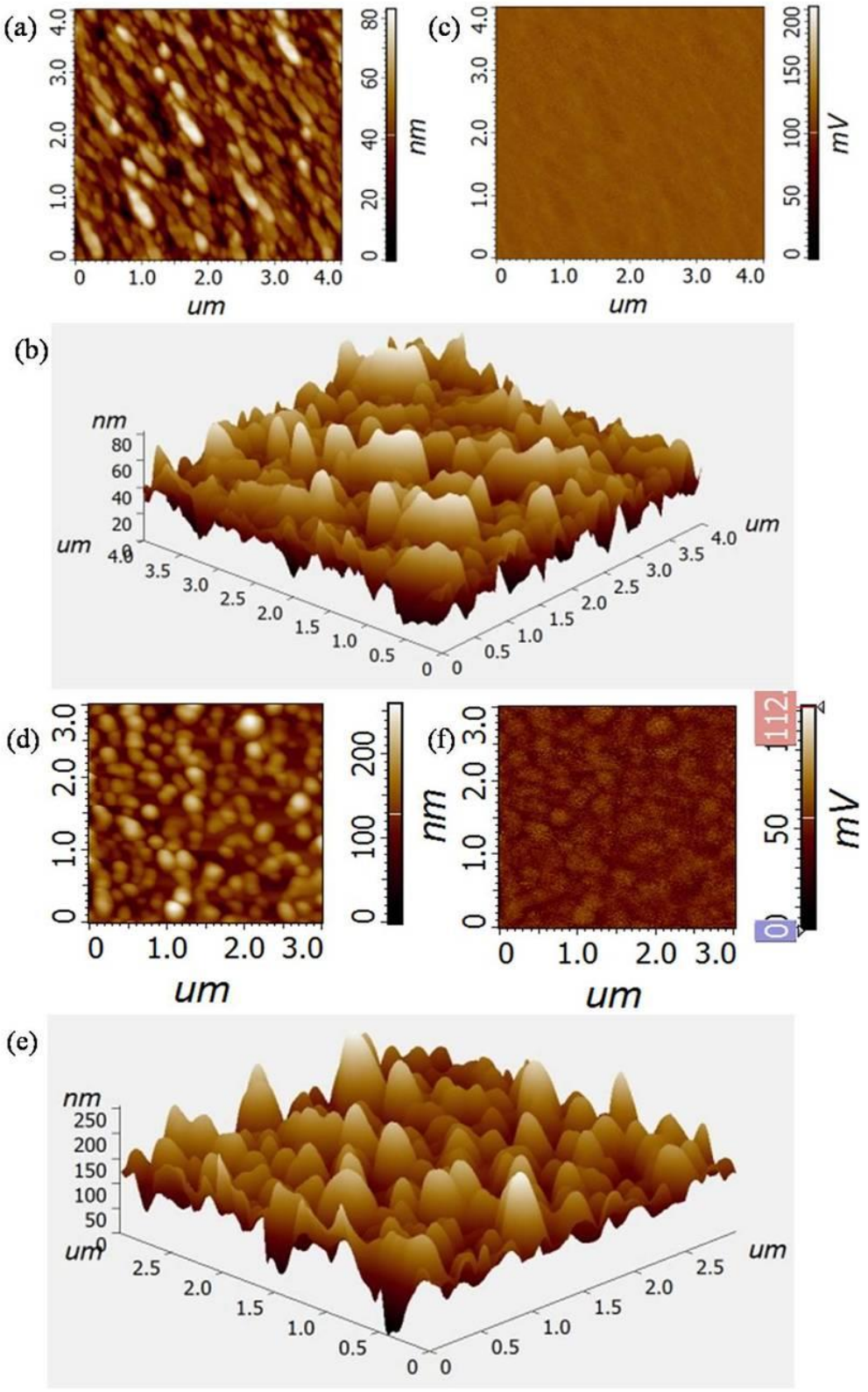

Figure 6.7 AFM image of pure PIn (a) and Fe-OEP/PIn(d), 3D image in (b) and (e), and KPFM in (c) and (f) respectively.

6.3.3 Electrochemical properties analysis:

The electrochemical properties evolution of Fe-OEP/PIn is investigated via CV and EIS technique. As shown in Figure 6.8 the comparative CV of Fe-OEP/Pin with pure PIn at scan rate 50 mV/sin potential range of 0-1.0 V. Non-aqueous 0.1M TABP in acetonitrile is used as electrolyte. In this, we prepared 1 mg/ml solution of Fe-OEP/PIn hybrid and PIn in THF and 5 µL solutions was used to modify the GCE by drop casting to study the electrochemical properties. The CV of Fe-OEP/Pin composite shows the enhancement in current as compare to pure PIn. Also shift of redox peak toward lower potential for hybrid material showing fast and easy movement of electrons.

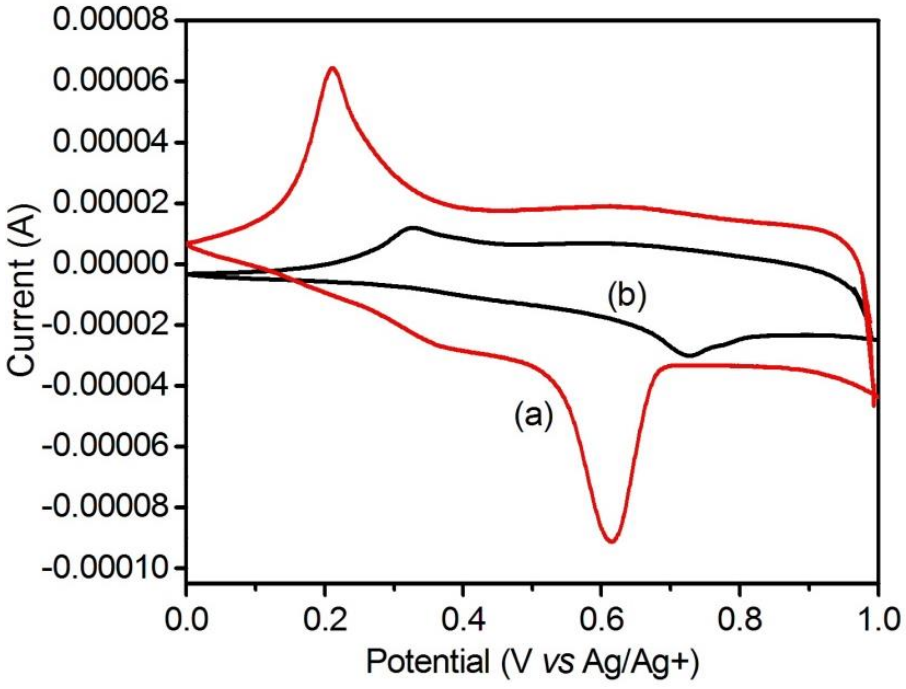

Figure 6.8 CV of (a) Fe-OEP/PIn hybrid and (b) pure PIn respectively.

The observed enhancement in current of Fe-OEP/PIn can be justified via synergic support between Fe-OEP and polymer backbone where charge transfer occurs. Meanwhile, Fe-OEP provide a centre for redox and polymer chain facilitate to transport this electron through polymer matrix the charge transport and resulting a good current as compare to pure PIn. This results indicated the Fe-OEP/PIn have higher specific capacitance over the pure PIn.

To understand the electrochemical behavioral of as prepared samples, EIS measurements were carried out at OCP of the same materials in similar condition as for CV. Figure 6.7 shows the nyquist plots of Fe-OEP/PIn hybrid and PIn (inset represents the zoom portion), which consists of depressed semicircle at high frequency region and a straight line at low frequency region. Semicircle at high frequency region is showing charge transfer resistance (Rct), if diameter of semicircle is high, it means the electrode associate with higher Rct. The straight line at low frequency region defined the ion diffusion resistance within the electrode materials [Chulliyote et al. (2017)]. Generally, the more vertical straight line is indication of the more capacitive behavior [Wang et al. (2016)]. Fe-OEP/PIn hybrid has much lower charge transfer resistance, and is showing the vertical straight line with more inclined towards the imaginary axis (Figure 6.9a). However, nyquist plot corresponding to PIn gives a semicircle at high frequency region and very high ion diffusion resistance (*see* Figure 6.9b) which is expected due to its compact structure. These EIS niquist plot result are in good agreement with CV data and suggested the Fe-OEP/PIn hybrid have better electrochemical performance over PIn.

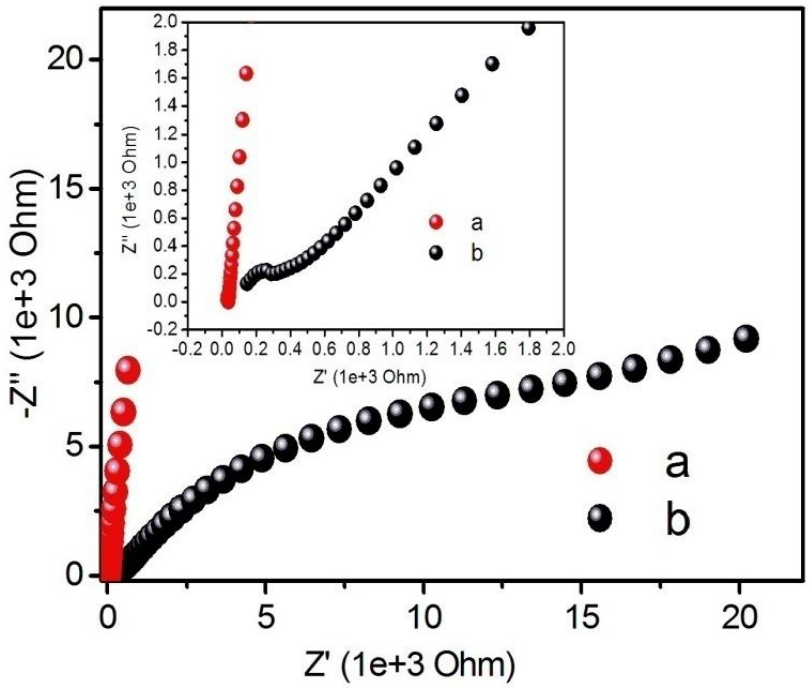

Figure 6.9 Nyquist plot of (a) Fe-OEP/PIn and (b) pure PIn respectively.

As a proof of concept, the electro-active, porous and networks structured is a promising material for supercapacitor. Therefore, prepared hybrid is explored as electrode material for supercapacitor.

Supercapacitive performance of Fe-OEP/PIn hybrid

To perform super-capacitive performance studies, the modified glassy carbon electrode (GCE; of diameter 3.0 mm) was fabricated follow similar protocol of chapter 3 (for details *see* 3.2.4). Figure 6.10 exhibits the galvanostatic charge-discharge (GCD) curves of the Fe-OEP/PIn-based electrodes at different current densities in 1.0M H_2SO_4 electrolyte. GCD curve have consistency in their shape under dissimilarity in the current density, which indicating the good reversibility of electrode materials. The specific capacitances calculated at different current density,

according to the discharge curves (as Figure 6.10) is 338.42, 326.4, 99.3, 303.1, 265.9 and 119.1 F/g with help of equation:

$Cs = \Delta t \times I / (\Delta V \times m)$

Where Δt is the discharge time, I is applied current density, ΔV is voltage range, and m is the mass of the electrode material [Chen et al. (2015), Shayeh et al. (2018)].

The GCD curves shows that a non-triangular shape, which implying that Fe-OEP/PIn exhibited a reversible psudocapacitive property.

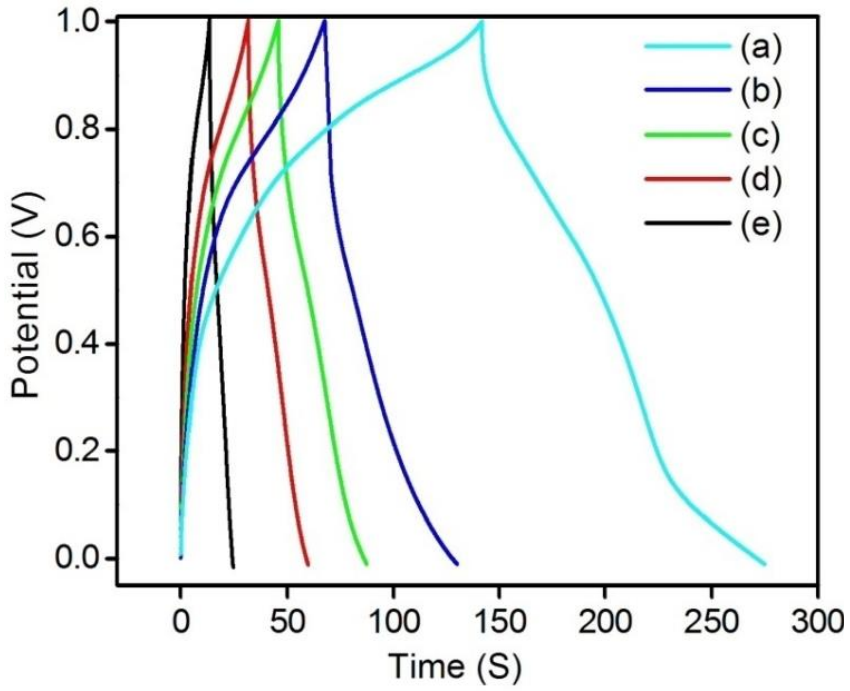

Figure 6.10 GCD of Fe-OEP/PIn at different current density as as (a) 2.5A/g, (b) 5A/g, (c) 7A/g, (d) 9A/g and (e) 10A/g respectively.

Further cyclic stability test of Fe-OEP/PIn has performed by repeating 7 cycles as shown in Figure 6.11. GCD curves showing almost similarity in their shapes which is depicted that such electrode is stable and have retain in their performance over the multi-cycles.

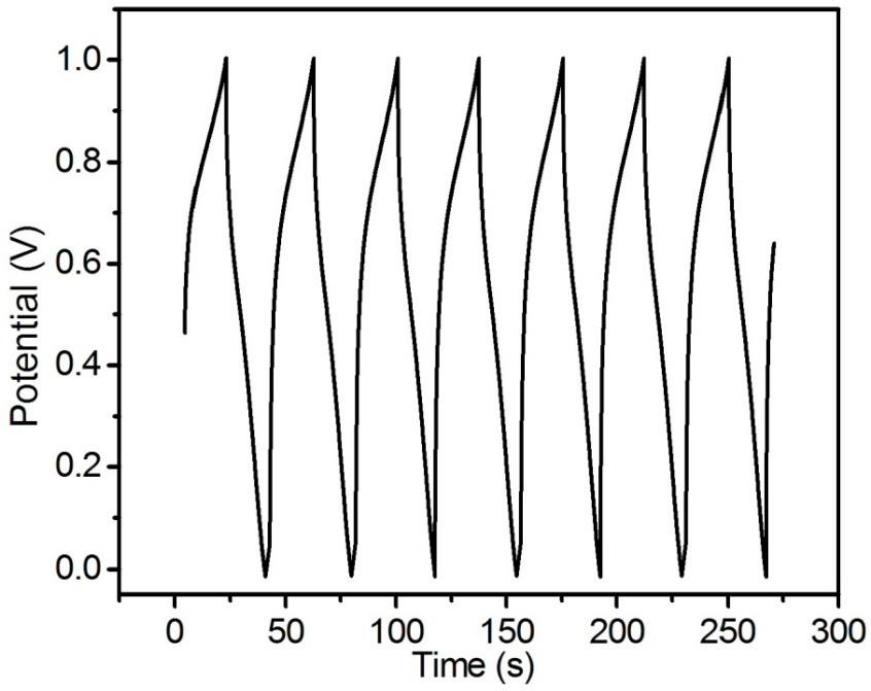

Figure 6.11 GCD cyclic stability test of FeOEP/PIn at current density 9A/g.

6.3.4 Conductivity and Charge transport Studies

The charge transport property of Fe-OEP/PIn hybrid was interrogated using the sandwiched structure of Al/Fe-OEP-PIn/ITO. Prior to fabrication of device, ITO was washed by double distilled water, ethanol and sonicated in acetone for half an hour. A solution of Fe-OEP/ PIn composite (1 mg/mL) in THF was used as initial solution for deposition of film. The film was deposited using spin coater at speed 800 rpm for successive deposition of 10 layers. The film was dried after every deposition at 60 °C for 10 min. Second electrode aluminium of 120 nm thickness was deposited over film with shadow mask of TEM grid of mess size 100 μm×100 μm using thermal evaporation at ∼10−6 mbar chamber pressure. The thickness of electrode was monitored by digital thickness monitor (DTM) unit equipped with quartz crystal microbalance.

The charge transport properties of Fe-OEP/PIn, and parameter of electronic device was extracted using sandwiched structure of Al/Fe-OEP/PIn/ITO and investigated using J–V measurements, semilog plot and $J^{1/2}$ vs. V at room temperature (27 °C) in air under dark condition as shown in Figure 6.12. It is important to note that Schottky diode formation takes place when work function of metal is less than work function of polymer (for p type semiconducting polymer). According to this theory, the J–V relationship for Schottky diode (also called Shockley Diode equation for diode) is expressed in literature [Pandey et al. (2014), Singh et al. (2017), Pandey et al. (2013), Singh et al. (2017)].

$$J = J_0\left[\exp\left(\frac{qV}{\eta kT}\right)\right] \quad \ldots\ldots\ldots\ldots\ldots\ldots\ldots\ldots\ldots\ (1)$$

where η is ideality factor and J_0 is the saturation current density in absence of external bias, q is electronic charge, V is the applied voltage, T is temperature in Kelvin and k is the Boltzmann constant. $J_0$is related to the Schottky barrier height, Φ_B as

$$J_0 = A^* T^2 \exp\left(\frac{-q\Phi_B}{kT}\right) \quad \ldots\ldots\ldots\ldots\ldots\ldots\ldots..(2)$$

where A* is the effective Richardson constant. The value of A* is calculated and found to be 120 A cm^{-2} K^{-2} by using effective mass of charge carrier and ΦB is the barrier height.

Or ideality factor

$$\eta = \frac{q}{kT}\left[\frac{\partial V}{\partial \ln(J)}\right] \ldots\ldots\ldots\ldots\ldots\ldots\ldots\ldots\ldots..(3)$$

Now for calculation of intrinsic mobility of hybrid materials as shown in table 1

Table 6.1: Electronic device parameters.

Device	J_0 (A/cm^2)	Φ_B (eV)	η	μ (cm^2/ Vs)
Al/FeOEP-PIn/ITO	1.17x10^{-3}	0.604	2.1	0.21

$$J = \frac{8}{9}\varepsilon_o\varepsilon_r\mu_h\frac{v^2}{d^3} \quad \text{.....(4)}$$

where, ε_0 is permittivity of free space, ε_r is relative permittivity and its value is ~3 for conducting polymer. 'd' is thickness of film or separation of electrode which is 200 nm. Based on the above equations and Figure 6.12(a–c), we calculated the intrinsic mobility μ_h (Eq. (4) and Figure 6.12c) saturation current density J_0, barrier height ΦB and ideality factor η (Eq. (2) and Figure 6.12b) of devices and given in Table 6.1. The ideality factor of device is 2.1 showing deviation from ideal diode. This indicates that the ideality factor does not only depend on interface phenomena in polymer but also on the bulk property of semiconducting polymeric materials also. Further, the current density is much higher as compare to report one [7,50] and mobility calculated on the basis of Eq. (4), shows 0.21 cm^2/vs. The higher current and better mobility can be explained on the basis of SEM image, XRD, synergic and Mott's law of variable-range hopping for variety of disordered materials. SEM image shows the formation of flowery structure meanwhile structural characterization reveals the enhancements in crystallinity after hybrid formation. The crystalline nature of material facilitates the charge transport. It is noteworthy that presence of Fe-OEP between PIn polymer chains in crystallites of hybrid facilitates charge transport due to synergic effect. It is unlikely that the synergic support plays a significant part in this large increase in conductivity. This behaviour is indicative of percolative character in disordered

system. Percolation theory deals with the effect of varying the number of interconnections present in a random polymer system. In this case the interconnections are Via Fe-OEP.

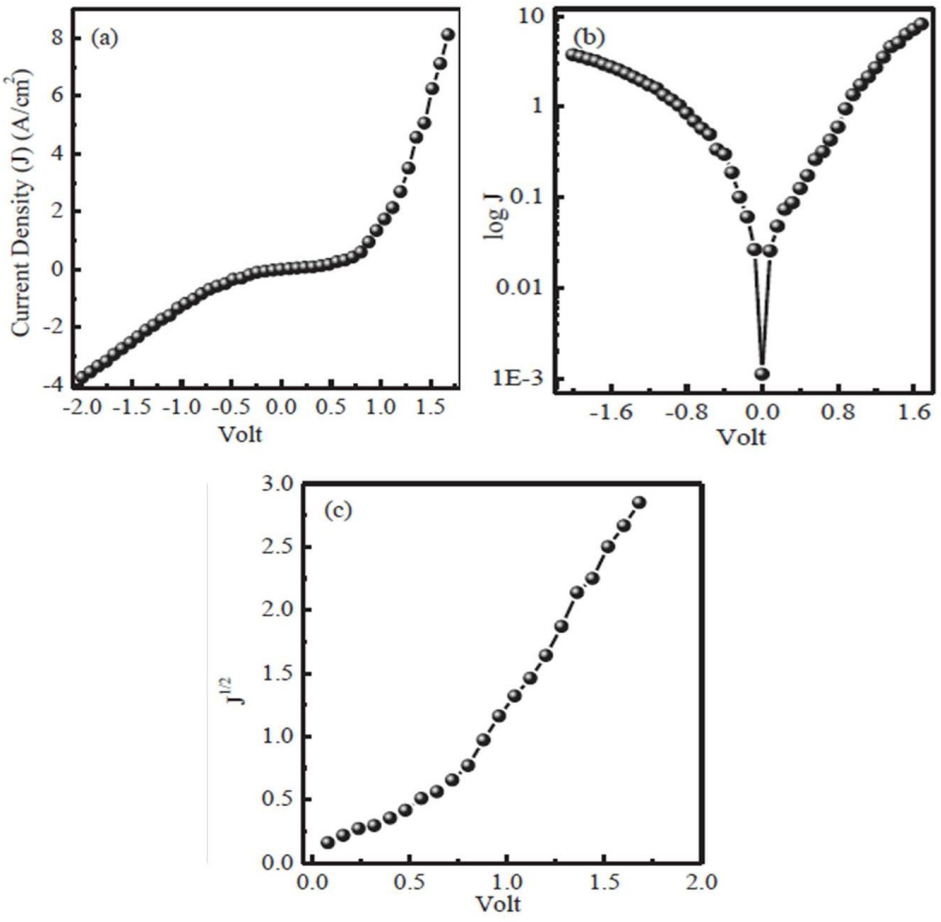

Figure 6.12 J-V (b) semilog plot (c) $J^{1/2}$ vs. V characteristics of Fe-OEP/PIn.

6.4 Conclusion:

We have reported one step in situ synthesis of Fe-OEP/PIn hybrid material for electrochemical supercapacitor as well as electronic applications where coordination of iron in OEP occurs at room temperature. The absorption spectra reveal coordination of Fe in OEP, polymerization of indole and contemporarily formation of

Fe-OEP/PIn hybrid materials. Further, the as formed hybrid was investigated via NMR, XPS, and FT-IR which again confirms the same. Structural characterization using XRD reveals the formation of crystalline/ordered materials with appearance of some sharp peaks. The electrochemical study of hybrid material reveals significant enhancement in electro activity as well as conductivity as compared to pure PIn. The specific capacitances Csp for Fe-OEP/PIn hybrid was obtained 338.42 F/g at 2.5 A/g current density. Further, the charge transport properties of hybrid was investigated using Al/Fe-OEP/PIn/ITO configuration showed 0.21 cm^2/Vs mobility (μh), 2.1 ideality (η) factor, and 0.60 eV barrier height (ΦB).